Small particle size distributions from mobility measurements

T. M. Sanders, Jr. and S. R. Forrest
H. M. Randall Physics Laboratory, The University of Michigan, Ann Arbor, Michigan 48109-1120

(Received 13 April 1989; accepted for publication 13 June 1989)

We report experiments performed on iron particles with radii in the range 40–100 Å, produced by pulsed evaporation from an electroplated tungsten filament in a cryogenic helium gas atmosphere. Flight times in electric fields of singly charged particles produced in the evaporation process yield values for gas velocity and charged particle mobility. Particle size distributions are determined both by electron microscopy and from the mobility. The latter method yields particle size distributions quickly and with good statistics, but with indicated radii larger by about 20 Å than those determined by electron microscopy. The discrepancy, which is most important for the smallest particles, is attributed to the effect of van der Waals interaction between the iron particles and the gas atoms. Comparison is made with theory, which connects the van der Waals interaction with the dielectric response functions. For particles in this size range, a van der Waals interaction determined from *bulk* iron data gives a satisfactory explanation of the discrepancy.

I. INTRODUCTION

Several different techniques have been employed to determine size distributions of submicrometer particles. In the course of experiments in which we produced iron particles by pulsed evaporation from an electroplated tungsten filament in an inert gas atmosphere,[1,2] we decided to study the particles which might become charged in this process. In these experiments the temperatures are too low and the particles are too small for there to be appreciable numbers of iron particles lacking electrons. There will, however, be electrons and positive alkali impurity ions emitted by the filament; we anticipated that we might be able to detect particles with both signs of charge. This has proved to be the case.

In this paper we will describe the experiments we performed, particularly on the positively charged particles. We will show that it is possible to use the time-dependent current waveform to determine the convective gas velocity and the mobilities of charged particles in the apparatus. These mobilities can be used to determine the particle size distribution. We prefer this method of determining size distributions to the other we have used, electron microscopy, because the distribution is available immediately, and better statistics are obtained with much less effort. There is, however, a small systematic difference between the sizes determined by the two methods, an effect we attribute to van der Waals interactions.

We will first describe the experimental apparatus, then give some data, present data reduction, and finally discuss the interpretation of the results and compare the present technique with others.

II. EXPERIMENT

A. General

In our experiments we have produced "smokes" of small particles of various metals by evaporating them from an electroplated tungsten filament (0.0127 cm diameter) in a helium gas atmosphere maintained at cryogenic temperature. The low temperature greatly reduced the tendency of the small crystals to aggregate into large clusters and chains, a striking phenomenon when the evaporations were performed at higher ambient temperatures.[3] We suspect that the aggregation process is thermally activated.[4] We have measured times of flight of charged iron particles in a sealed cell which is immersed in a pumped bath of liquid helium. The pressure of the helium gas in the cell was varied from approximately 0.5 to 10 Torr.

B. Source

The particles are produced by pulsed evaporation from a filament which is heated by a constant-voltage pulse approximately 250 ms long. The voltage drop across the filament is monitored by two potential leads, and an operational amplifier driver circuit provides a rectangular voltage wave form across the filament. An analog divider is used to determine the time-dependent resistance of the filament, a measure of the average filament temperature. Evaporation occurs from the hottest portion of the filament; we have related the filament "hot-spot" temperature with filament resistance by the use of optical pyrometry. Filament temperature, when referred to below, will indicate hot-spot temperatures determined by this two-step process. During filament firing, both ends of the filament are several volts positive with respect to ground; after firing, the filament is at ground potential. When the filament is fired, atoms are evaporated from the filament during the time the filament is hottest. The atoms travel out from the filament, losing their large initial velocity by colliding with the helium atoms and coalescing into larger and larger clusters. This process occurs in a spherical volume, typically about 1 cm in radius, which we call the ballistic region. Beyond the ballistic region the particle motion is determined by the flow velocity of the gas and by forces applied to the particles.

C. Electrodes

The charged particles are controlled and detected by the grids and collector shown in Fig. 1. The source grid is placed

 0021-8979/89/193317-07$02.40

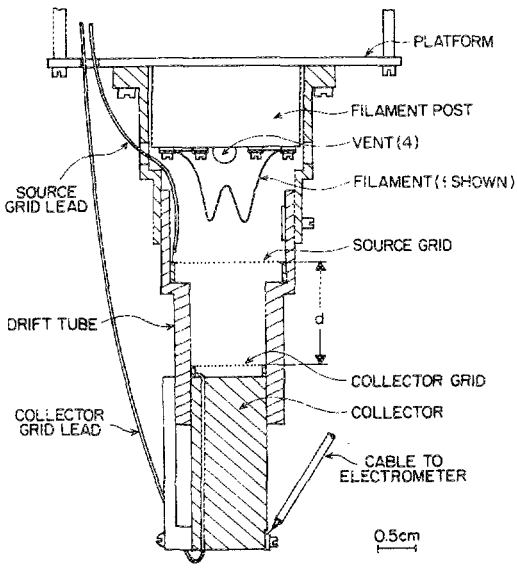

FIG. 1. Cross section of cell for measurement of charged particle transit times in helium gas atmosphere.

just outside the ballistic region. The potential of the source grid is usually set equal to that of the midpoint of the filament by using a voltage divider. The space between the two grids is called the drift region; its length d is set to 1.2 or 1.6 cm. Both grids were fabricated of gold with 8 lines/cm and transmission near 95%. Below the collector grid by 1.8 mm is a copper collector plate connected to an operational amplifier electrometer with sensitivity near 0.5 pA and a response time of approximately 10 ms. Grid and collector potentials can be varied to set the magnitudes and signs of the electric fields in the various regions.

D. Observations

We show in Fig. 2 a typical electrometer output when the potentials are adjusted to collect positive charges. When the potentials are set to collect negative charges, signals of larger magnitude and similar shape are observed. It would be interesting to study these negative particles also, but this was not done in the present experiments.

We have designated three features of the waveform as the prompt pulse, the trailing edge pulse, and the late pulse. We now discuss their causes. The prompt pulse appears during the filament heating period. We associate it with collection of alkali impurity ions evaporated from the filament. Both potassium and sodium are volatile materials whose vapor pressure varies approximately as $\exp(-5000\ \mathrm{K}/T)$; potassium is present in the tungsten wires, and sodium is a likely contaminant in our electroplating and handling procedures. The approximate mobility of a K^+ ion under the conditions of Fig. 2 would be 300 $\mathrm{cm}^2/\mathrm{V\ s}$, and its time of flight is small. The calculated evaporation rate for K or Na is plotted against time in Fig. 3(a). Its similarity to the observed prompt pulse supports this identification. We interpret the narrow pulse which appears at the trailing edge of the firing pulse as a current due to emission of photoelectrons from the copper collector. This identification is suggested by the fact

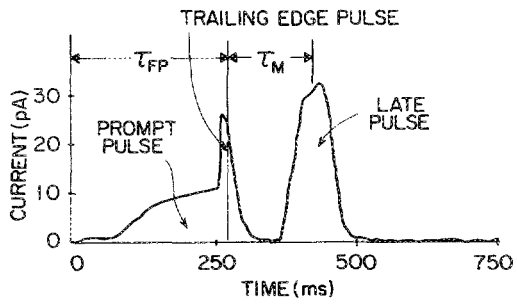

FIG. 2. A typical electrometer output when the potentials are adjusted to collect positive charges. The time τ_{FP} is the duration of the filament firing pulse. Time τ_M is a transit time, measured from the end of the firing pulse.

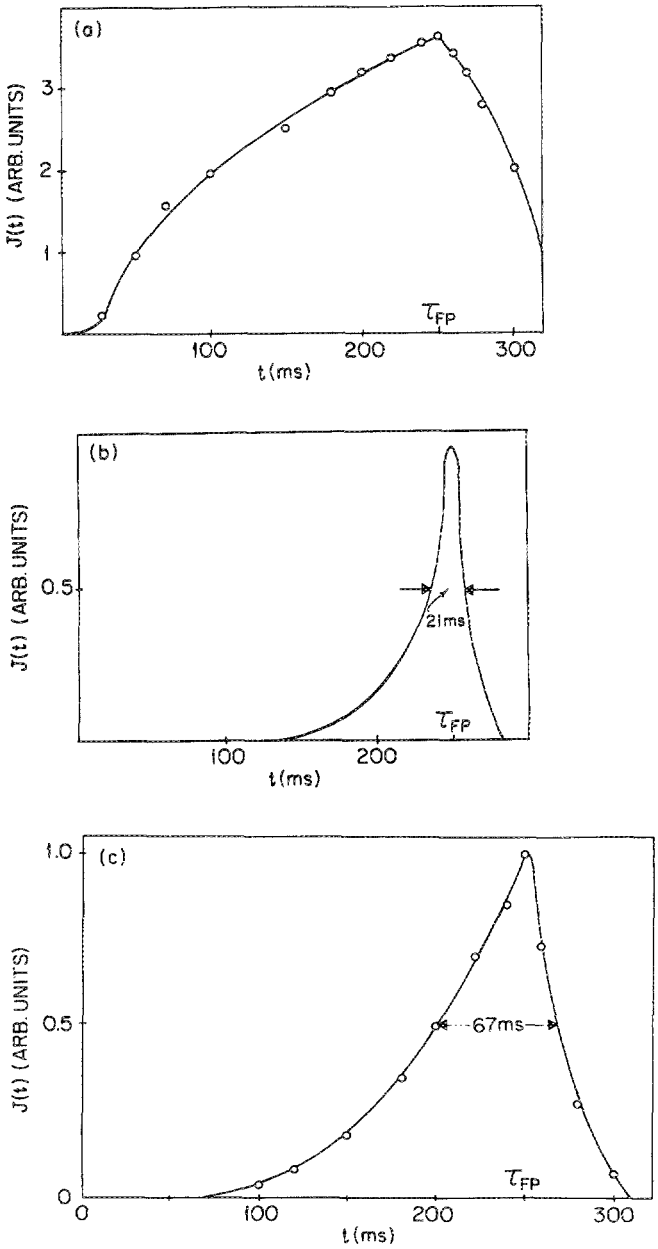

FIG. 3. (a) Calculated evaporation rate for K or Na plotted against time. (b) Calculated flux of photons with energy greater than 4.5 eV plotted against time. (c) Calculated evaporation rate of iron.

that the magnitude and timing of this pulse are unaffected by the electric field in the drift region. Additional support of this identification is provided in Fig. 3(b) where we show the calculated flux of photons with energy greater than 4.5 eV plotted against time. The magnitude of the current is consistent with this model if the quantum yield of the collector is approximately 4×10^{-3}. Both the prompt pulse and the trailing edge pulse are observed with bare tungsten filaments. The late pulse is observed only with plated filaments heated to at least 1600 K. We associate it with collection of positively charged iron particles. Since the evaporation rate of iron is a rapidly varying function of filament temperature, approximately proportional to $\exp(-20\,000\,\mathrm{K}/T)$, evaporation occurs primarily near the end of the heating pulse. We show the calculated evaporation rate of iron in Fig. 3(c). The evaporation rate peak has a full width at half maximum of 67 ms; the observed late-pulse widths are sometimes as small as 35 ms. The additional narrowing may occur because clusters form only at the highest vapor densities, but we have not studied the effect in detail. At any rate, it should be a good approximation to take the creation time of a cluster to coincide with the end of the heating pulse. Multiply charged particles should have mobilities proportional to their charges, and correspondingly earlier arrival times. We see no evidence of such early arrivals nor would they be expected for energetic reasons. In the analysis which follows we will assume all charged particles to be singly charged and to be created at the end of the heating pulse.

III. DATA ANALYSIS

A. Methods

The average motion of particles of mobility μ in electric field $\mathbf{E}$ in a gas with flow velocity $\mathbf{v}_g$ relative to the laboratory is given by

$$\mathbf{v} = \mathbf{v}_g + \mu\mathbf{E}. \tag{1}$$

We will assume, for the moment, that $\mathbf{v}$, $\mathbf{v}_g$, and $\mathbf{E}$ are all in the same direction and independent of position, whence

$$v = v_g + \mu E. \tag{2}$$

The particle velocity v approaches v_g when $\mu E \ll v_g$. We determine v_g in two ways: A series of filament firings is taken under identical conditions except that the electric field E is changed. The gas velocity is found by extrapolating the drift time (and velocity) to zero field, i.e. $v_g = \lim_{E\to 0} v$.

The second method permits determination of v_g from a single firing. If, at the electric field values used, there are particles with mobility so low that $\mu E \ll v_g$, the transit time of the slowest particles $t_{\max}$ will determine v_g by $v_g = d/t_{\max}$. This second method is preferred because it is not necessary to assume that v_g is completely reproducible between firings. The two methods are generally in good agreement. See Fig. 4, a plot of the field dependence of the velocity of the particles at the pulse peak and of the slowest particles, for a series of firings at $p = 0.9$ Torr, $T = (2.6 \pm 0.3)$ K.

The mobility of a singly charged heavy particle in a light gas when the particle size is small compared to the mean free path of the gas molecules is[5]

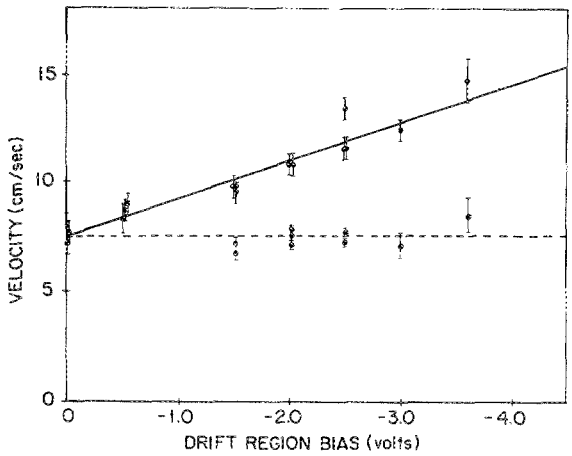

FIG. 4. Field dependence of the velocity of the particles at the pulse peak (solid line) and of the slowest particels (dashed line).

$$\mu = C(p,T)/Q^{(1)}, \tag{3}$$

with

$$C(p,T) \equiv (3e/16p)(2\pi RT/\mu_g)^{1/2}. \tag{4}$$

Here e is the electron charge, p the pressure, T the temperature, μ_g the molecular weight of the gas, and $Q^{(1)}$ is the momentum-transfer cross section, which is related to the differential cross section for scattering of a gas atom by

$$Q^{(1)} = \int \left(\frac{d\sigma}{d\Omega}\right)(1-\cos\theta)d\Omega. \tag{5}$$

In our experiments all quantities determining μ are known except the cross section. Thus a measurement of μ determines $Q^{(1)}$ and an effective particle radius a_μ, which we define by $Q^{(1)} \equiv \pi a_\mu^2$. We may relate the transit time t through a drift space of length d with potential difference V to particle radius a_μ by writing

$$d/t = v_g + [C(p,T)V/\pi a_\mu^2 d]. \tag{6}$$

From this we obtain

$$a_\mu = [C(p,T)Vt/d\pi(d - v_g t)]^{1/2}. \tag{7}$$

The measured quantity is the time-dependent current $i(t)$. The quantity $i(t)dt/e$ is the number of singly-charged particles collected in the interval from t to $t + dt$. We equate this to $g(a_\mu)da_\mu$, the number of particles with radius between a_μ and $a_\mu + da_\mu$, and obtain

$$g(a_\mu) = i(t)/(e\, da_\mu/dt), \tag{8}$$

which can be expressed in terms of measured quantities by differentiation of the expression (7) for a_μ.

B. Results

We show in Fig. 5 the size distribution $g(a_\mu)$ derived from the late pulse shown in Fig. 2. Note that the size distribution is quite unsymmetrical. The peak of the distribution is at $a_{\mu p} \cong 50$ Å; the median radius is $\bar{a}_\mu = (58 \pm 4)$ Å. The median radius averaged over electric field values at this temperature and pressure is (64 ± 5) Å. Similar distributions can be obtained at various pressures and temperatures. We have measured $a_{\mu p}$ at three different pressures at $T = 2.6$ K.

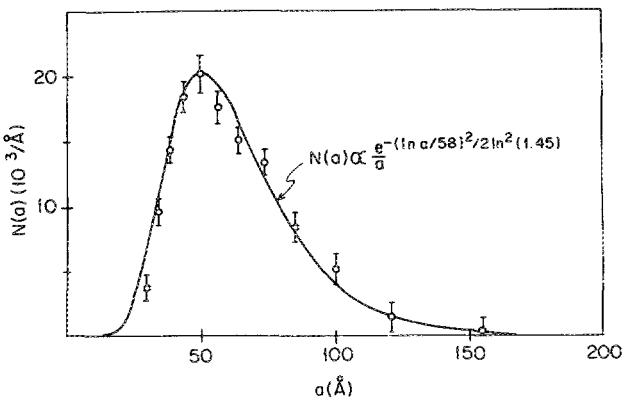

FIG. 5. Size distribution $g(a_\mu)$ derived from the late pulse shown in Fig. 2. The solid line is a log-normal distribution with parameters shown.

The resulting values are fitted roughly by a power law $a_{\mu p} \propto p^{(0.15 \pm 0.05)}$.

IV. DISCUSSION

A. Comparison with other methods

Size distributions of particles produced by evaporation in inert gas atmospheres have been studied by other workers.[6] A technique frequently used is to collect the particles on a thin film and subsequently study the deposited particles in a transmission electron microscope. We have performed such studies in our apparatus, and show a typical particle size distribution in Fig. 6. In order to obtain this distribution, the filament was fired 10 times; the apparatus was warmed to room temperature; the grid supporting the thin carbon film holding the deposit was transferred to the electron microscope; a photograph was taken and processed, and a section of the photograph was scanned; size measurements were performed on approximately 250 particles. Results were not available until several days after the run.

An extensive study of particle size distributions determined by electron microscopy has been reported by Granqvist and Buhrman,[7] whose size distributions are well approximated by the log-normal function

$$g(a) = \frac{N_{\text{tot}}}{a\sqrt{2\pi}(\ln\sigma)^2} \exp\left[-\frac{1}{2}\left(\frac{\ln(a/\bar{a})}{\ln\sigma}\right)^2\right]. \quad (9)$$

The smooth curves shown in Figs. 5 and 6 are fitted log-normal distributions. Best-fit median radii $\bar{a}$ and dimensionless width parameters σ are shown. Our size distributions, determined by electron microscopy and by the mobility technique, are both fitted quite well by the log-normal form. The slow increase of particle radius with inert gas pressure has also been noted by other workers.[8] The data of Granqvist and Buhrman are consistent with $a \propto p^{0.3}$. Our radii determined by electron microscopy show a similar behavior, $\bar{a}_{\text{em}} \propto p^{(0.33 \pm 0.19)}$, but the charged-particle radii determined by the mobility method are systematically larger and more slowly varying with pressure $a_{\mu p} \propto p^{(0.15 \pm 0.05)}$, as was discussed in Sec. III B.

The use of charged particle mobilities to characterize particle size distributions has been pioneered by Whitby *et al.*[9] Since they study initially neutral particles, their apparatus includes a charging region utilizing an electric discharge. They measure a steady current in the presence of a known flow velocity and a transverse electric field. The configuration is very different from the present one and analysis of the results is complicated by multiple charging, which occurs in the discharge region. In the present experiments, both theory and experiment indicate that there is insufficient energy to produce multiple charging, except perhaps for particles so large that both their number and mobility are unmeasurably small. The mobilities in the present experiments are three orders of magnitude larger than those encountered by Whitby *et al.* The largest particles we study have sizes comparable to the smallest studied by them, so the techniques are complementary.

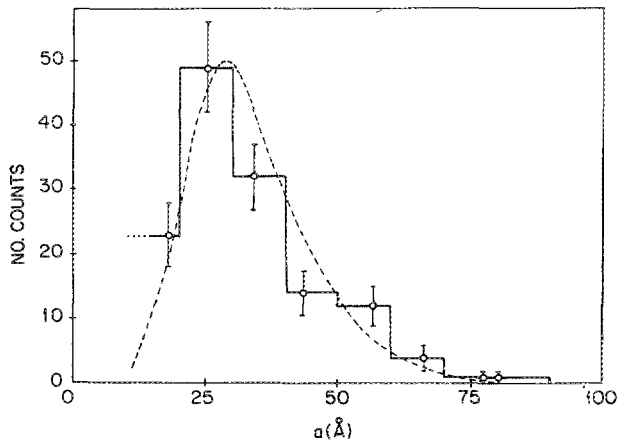

FIG. 6. A typical particle size distribution obtained using a transmission electron microscope. The dashed line is a log-normal function with parameters $\bar{a} = 35$ Å, $\sigma = 1.4$.

B. Interpretation

We have noted a systematic difference between the particle distribution determined by electron microscopy and the distribution inferred from mobility measurement of positively charged particles. Before concluding that this difference is real we turn to the matter of systematic errors which may influence our determination of particle size from mobility.

We have previously described a number of assumptions and idealizations used in the analysis of our data. These certainly preclude use of this method for high-precision determination of particle size distributions. We now show, however, that the discrepancy with particle sizes determined by electron microscopy is much too large to be explained by these effects.

1. Systematic errors in measurements

We have assumed that the particles appear at the start of the drift region, precisely at the end of the filament firing pulse, and that the gas flow field in which they move is independent of space and time. We have already discussed the actual distribution of "birth times" of the particles due to the time dependence of the evaporation rate of the iron. Since we

have observed pulses as narrow as 35 ms, it seems unlikely that these effects can be larger than 30%. In order for the true radius to be smaller than the apparent one, the true mobility would have to be larger, and the true transit time shorter; thus the particles would have to be "born" *after* the end of the firing pulse, which seems very unlikely. After the atoms are emitted from the filament, a finite time is required for them to coalesce into crystallites, and for the crystallites to slow down with respect to the gas. These processes are difficult to analyze precisely, but the time required for the particles to slow down can be estimated from the measured mobilities. The characteristic time τ can be estimated from $\tau = m\mu/e \cong 10^{-6}$ s, for typical particles with $\mu \cong 3$ cm^2/V s and $a \cong 60$ Å ($N_{\rm Fe} \cong 10^4$). This time and also estimated clustering times are orders of magnitude too small to be significant in our experiment, where we deal with transit times of order 10^{-1} s.

The assumption that the particles come to rest precisely at the entrance to the drift region is also not accurate. It is easy to show, however, that if the particles come to rest in the source region, then the plot of velocity versus electric field will become nonlinear. Experiment (see Fig. 4) rules out any large nonlinearity. One has for the apparent velocity v_a

$$v_a \equiv d/t_t = d/[\delta/v_g + d/(v_g + \mu E)] \tag{10}$$

if the particles start a distance δ before the drift region. If, on the other hand, the particles come to rest within the drift region the apparent mobility will be *greater* than the true one, and the apparent size will be *smaller* than the true one. Neither possibility explains our discrepancy.

The gas flow velocity in the cell is not precisely constant. However, variation in flow velocity across the charged-particle beam would result in a broadening of the beam, and no such phenomenon is observed. A variation along the beam is expected, and its consequence is easily analyzed if the variation is linear. We find

$$v_a = d/t = [v_g(d) - v_g(0)]/\ln[v(d)/v(0)], \tag{11}$$

leading to an apparent weak-field mobility given by

$$\mu_a \equiv \frac{d}{dE}\frac{d}{t} = \mu(1-x)^2/(x\ln^2 x),$$

where

$$x \equiv [v_g(d)/v_g(0)]. \tag{12}$$

This correction is negligible except in extreme cases where x is very different from 1. In such cases this effect will (i) always *raise* the apparent mobility above the true one, leading to an *underestimation* of the radius, and (ii) produce a nonlinear dependence of v_a upon E. We conclude that we cannot find an experimental error of the magnitude and sign required to explain our discrepancy.

2. Connection between cross section and radius

(a) We have defined an effective radius a_μ by $Q^{(1)} = \pi a_\mu^2$. For hard sphere collisions, a_μ is the sum of the radii of the colliding objects. The radius of a He atom[10] is approximately 1.5 Å, so that for particle radii greater than 30 Å the difference between particle radius and a_μ due to this cause is never more than 5%.

(b) There will be helium atoms adsorbed on the metal particle under the conditions of our experiments. Estimates of the thickness of the adsorbed layer under our conditions (which are time dependent after the filament is flashed) give thicknesses of approximately 5 Å for a true particle radius of 40 Å. Such an effect may be marginally detectable, but is small compared with the discrepancy between the two methods of determining particle radii.

(c) Deviations from hard-sphere scattering will alter the connection between particle radius and cross section. If the scattering were primarily backward, the effective radius might be larger than the geometrical value by a factor up to $\sqrt{2}$. Forward scattering will correspondingly reduce the effective radius below geometrical. If the atoms are absorbed into the film and subsequently emitted isotropically and elastically, the result is identical with hard sphere scattering. If the atoms are diffusely reflected upon collision, the cross section is greater than the geometrical by a factor of 13/9. None of these mechanisms explains the discrepancy.

(d) There are long-range interactions between the charged particle and the colliding atom. These can sometimes have significant consequences. The electrostatic (polarization) energy, $|V_\alpha| = \frac{1}{2}\alpha(0)E^2$ is negligible compared with $k_B T$ under the conditions of the present experiment.[11] For a single electronic charge and radii greater than 30 Å, $|V_\alpha|/k_B < 0.02$ K. The van der Waals interaction, on the other hand, can produce surprisingly large effects, which we now estimate.[12,13] For an atom a distance d above a semi-infinite medium, the interaction is $V(d) = -\zeta/d^3$, while at large distances r from the center of a sphere it is proportional to r^{-6}. We model the potential as a function of r by

$$V(r) = -8\zeta a^3/(r^2 - a^2)^3 \quad \text{for} \quad r > a,$$
$$V(r) = \infty \quad \text{for} \quad r < a \tag{13}$$

and use the Lifshitz theory[14] to estimate ζ, finding quite consistent values at large and small values of r. This theory enables us to express ζ in terms of the dielectric response functions of the atom (He) and the substrate (Fe). We characterize iron by a single plasma frequency ω_p, so that

$$\epsilon_{\rm Fe}(\omega) = 1 - \frac{\omega_p^2}{\omega^2 + i\omega\gamma} = 1 + \frac{\omega_p^2}{s^2 - s\gamma}, \tag{14}$$

with $\omega = is$ and use for the frequency-dependent polarizability of a helium atom

$$\alpha_{\rm He}(\omega) = \frac{e^2}{m}\sum_n f_n/(\omega_n^2 - \omega^2). \tag{15}$$

The sum is over excited states of the atom. Following Sabisky and Anderson,[15] we include three terms in the sum: The most important bound excited state ($1s2p\ ^1P_1$) of He is at $\hbar\omega_1 = 21.2$ eV, and has an oscillator strength[16] $f_1 = 0.28$. We put the remaining one-electron oscillator strength ($f_2 = 0.72$) at the first ionization energy $\hbar\omega_2 = 24.6$ eV, and take the second electron oscillator strength ($f_3 = 1.0$) at the second ionization energy $\hbar\omega_3 = 79$ eV. We use[17] $\omega_p = 25$ eV for Fe, and find $8\zeta \cong 3.0\times10^4$ K Å^3, both for $r \gg a$ and for $r - a \ll a$. A natural energy unit for the scattering problem is $E_0 \equiv 8\zeta/a^3 = 0.24$ K for $a = 50$ Å. The scattering can be considered to be classical, since typical angular momenta are

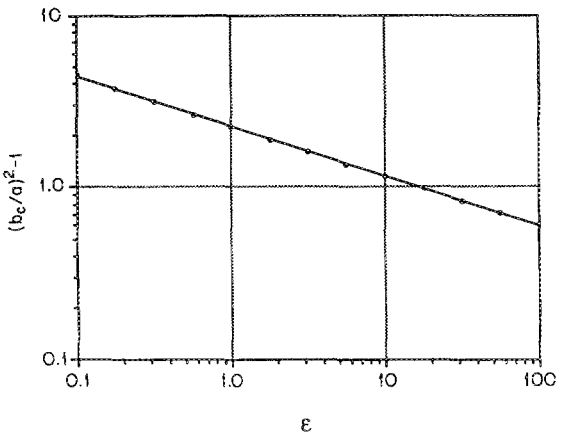

FIG. 7. Universal plot of $b_c^2/a^2 - 1$ vs $\epsilon \equiv E/(8\zeta/a^3)$. The quantity b_c is the critical radius for capture, a the geometrical (hard-core) radius. The line shows the power law $b_c^2/a^2 - 1 = 2.2556\,\epsilon^{-0.288\,65}$.

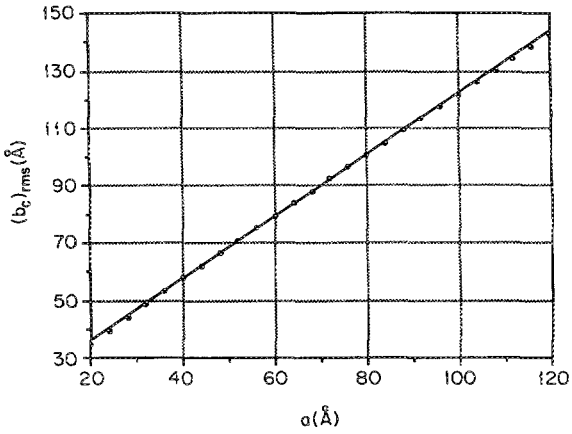

FIG. 8. Calculated radius $(b_c)_{rms}$, averaged over the Maxwell–Boltzmann distribution at $T = 2.6$ K, plotted against the geometrical radius a. The straight line shown, $(b_c)_{rms} = 1.0757a + 14.402$ Å, fits the data rather well in this range.

of order $a\cdot\sqrt{(3mk_BT)}/\hbar \cong 50$ under the conditions ($T \cong 2$ K) of our experiments.

For the model potential (13), deflections are small for impact parameters significantly greater than a critical value b_c, while for $b < b_c$, trajectories strike the sphere, resulting in large angular deflections. We approximate the momentum transfer cross section by πb_c^2. We show the dependence of b_c on energy in Fig. 7, which is a plot of $b_c^2/a^2 - 1$ vs $\epsilon \equiv E/E_0$. This is a "universal" plot, applicable regardless of sphere radius and van der Waals force constant. The points are fitted very well by the power law, $b_c^2/a^2 - 1 = 2.2556\,\epsilon^{-0.288\,65}$, so that we can readily perform integrals over the Boltzmann energy distribution. The result can be written in the form[18]

$$\langle b_2^c\rangle/a^2 \cong Q^{(1)}/\pi a^2 = 1 + 0.5\,\Gamma(3 - 0.288\,65)2.2556(T/E_0)^{-0.288\,65}$$
$$= 1 + 1.072(2.6\text{ K}/T)^{0.288\,65}(a/40\text{ Å})^{-0.865\,95}(8\zeta/3.0\times 10^4\text{ K Å}^3)^{0.288\,65}. \quad (17)$$

We show in Fig. 8 the calculated radius $(b_c)_{rms} \equiv \sqrt{\langle b_c^2\rangle}$ vs radius a. The relationship is very similar to that found experimentally between a_μ and a_{em}. We do not have data taken by the two methods under identical conditions. However, we find $\bar{a}_{em} = (44 \pm 4)$ Å at $p = 0.9$ Torr, $T = 1.6$ K and $\bar{a}_\mu = (64 \pm 5)$ Å at $p = 0.9$ Torr, $T = 2.6$ K. The agreement seems sufficiently good to allow the conclusion that the discrepancy between "mobility radius" and "electron microscope radius" is accounted for by the effect of the van der Waals interaction. To our accuracy we find no evidence that the van der Waals interaction for particles in this size range cannot be calculated from *bulk* properties. Furthermore, the fact that the fractional correction is largest for the smallest particles accounts, at least semiquantitatively, for the observation that a_{em} varies more rapidly with pressure than does a_μ.

V. CONCLUSION

We have demonstrated the usefulness of a mobility measurement for a real-time determination of particle size distributions in gas atmospheres. The distributions are available quickly and with good statistics. A discrepancy between apparent particle sizes determined by this method and by electron microscopy is attributed to effects of the van der Waals interaction between particles and gas atoms. This technique could permit accurate study of the dependence of the van der Waals force on particle size; our rather crude measurements find no discrepancy with bulk properties.

ACKNOWLEDGMENTS

This work received assistance from the Division of Materials Research, National Science Foundation and the Rackham School of Graduate Studies, University of Michigan. Parts of this paper were written while one of us (T.M.S.) was a guest at the Istituto di Fisica, Università degli Studi, Florence, receiving support from the John Simon Guggenheim Memorial Foundation.

[1] S. R. Forrest, Ph.D. dissertation, University of Michigan, Ann Arbor, MI, 1979.
[2] A brief account has been given in T. M. Sanders, Jr. and S. R. Forrest, Bull. Am. Phys. Soc. **26**, 563 (1981).
[3] S. R. Forrest and T. A. Witten, Jr., J. Phys. A **12**, L109 (1979).
[4] We are indebted to H. McConnell for this suggestion.
[5] E. W. McDaniel and E. A. Mason, *Mobility and Diffusion of Ions in Gases* (Wiley, New York, 1973).
[6] N. Wada, Jpn. J. Appl. Phys. **6**, 553 (1967); K. Kimoto and I. Nishida, Jpn. J. Appl. Phys. **6**, 1047 (1967).
[7] G. Granqvist and R. A. Buhrman, J. Appl. Phys. **47**, 2200 (1976).
[8] See Ref. 7.
[9] K. T. Whitby and W. E. Clark, Tellus **18**, 573 (1966).
[10] J. O. Hirschfelder, C. F. Curtiss, and R. B. Bird, *Molecular Theory of Liquids and Gases* (Wiley, New York, 1954), p. 203.

[11]We use the value 0.204 Å^3 for the static polarizability of a helium atom, $\alpha(0)$. See e.g., G. A. Cook, *Argon, Helium, and the Rare Gases* (Interscience, New York, 1961), p. 151.
[12]J. Gspann, Progr. Astronaut. and Aeronaut. **74**, 959 (1981).
[13]G. Akinci and J. A. Northby, Phys. Rev. Lett. **42**, 573 (1979).
[14]E. M. Lifshitz and L. P. Pitaevskii, in *Statistical Physics*, Vol. 9 of *Course of Theoretical Physics*, edited by L. D. Landau and E. M. Lifshitz (Pergamon, New York, 1980), Part 2, Sec. 82, p. 342.
[15]E. S. Sabisky and C. H. Anderson, Phys. Rev. A **7**, 790 (1973).
[16]W. L. Wiese, M. W. Smith, and B. M. Glennon, Eds., *Atomic Transition Probabilities*, National Standard Reference Data Series (National Bureau of Standards, Washington, DC, 1966), Vol. 1, p. 11.
[17]C. Wehenkel and B. Gauthé, Phys. Status Solidi B **64**, 515 (1974).
[18]Similar results have been obtained by Gspann (Ref. 12).